Journal of Thermal Analysis and Calorimetry, Vol. 97 (2009) 1, 191–196

SINTERING OF A NANO-CRYSTALLINE METASTABLE ALUMINA
Influence of the firing parameters on the phase development and microstructural evolution

Paola Palmero and M. Lombardi*

Department of Material Science and Chemical Engineering – Politecnico di Torino, INSTM Research Unit – LINCE Lab
Corso Duca degli Abruzzi 24, 10129 Torino, Italy

The influence of the heating rate on phase transformation and microstructural evolution during sintering of a de-agglomerated nanocrystalline, transition alumina was investigated. A low heating rate treatment allowed to decrease the α-Al_2O_3 crystallization temperature as well as to displace densification at lower temperatures, also implying a refinement of the fired microstructures. In addition, the set-up of sintering cycles in which the heating rate changed in the range 0.5–20°C min^{-1} starting from intermediate, selected temperatures resulted in a further retention of a very fine and homogeneous grain size in final materials.

Keywords: *microstructural evolution, nano-crystalline metastable alumina, sintering*

Introduction

Over the past 15 years, nanocrystalline oxide powders have become available from a variety of synthesis routes [1–3], but their processing to produce dense bodies retaining the nano-scaled structure has not proven easy. Frequently, the starting nanopowder is not the thermodynamically stable phase at the processing temperature, so that phase transformations occur during the densification process. A typical example is the transition alumina investigated in the present study. The transformation of nano-sized θ-alumina occurs through stages of nucleation and growth [4]; in the former, θ-Al_2O_3 crystallites reach a critical size and then transform to α-phase; in the latter, the transformation comes to completion through the coalescence of α-nuclei and their growth. The above described transformation is also accompanied by an increase of the theoretical density from transition to α-alumina and to the formation of a vermicular microstructure entrapping a relevant amount of intragranular, large pores [5, 6]. As a matter of fact, the final stage of sintering must be performed at very high temperatures to achieve full densification, but inducing a relevant grain growth [7].

Many attempts have been experienced to overcome the above limitation by increasing the material sinterability. Recently, the milling of a transition alumina was demonstrated to be effective in lowering its transformation temperature [8] and even in enhancing the densification by decreasing the α-alumina maximum sintering temperature [7].

The decrease of the transformation temperature was also successfully pursued by the addition of α-seeds, which can dramatically enhance the kinetics of the θ to α-Al_2O_3 transformation and significantly improve the microstructure of the transformed α-alumina [9]. The introduction of the α-Al_2O_3 seeds can be obtained through several routes, such as addition of suitable amount of α-alumina powder [5, 10, 11], high energy ball milling [12], prolonged ball milling with α-Al_2O_3 spheres as seeds source [11, 13] rapid heating of the powder at its transformation temperature, prolonged annealing or flash treatments of green bodies [6, 14].

Some innovative densification routes, such as master [15, 16], rate-controlled [17] and two-step [7, 18–20] sintering have been also exploited for increasing sinterability of nanopowders, demonstrating the effectiveness of new-designed thermal cycles on the control of grain growth in well-densified materials. Most studies are however devoted to compositions which do not undergo a phase transition during the thermal treatment, such as α-alumina, yttria, ZnO and α-alumina-based composites [15, 18]. On the contrary, if reference is made to transition aluminas, the above methods have not been systematically applied and only few data are present in literature [7].

Recently, the role of the dispersion of a commercial, nano-crystalline transition alumina powder on its compaction ability and sinterability has been clearly assessed and a very high densification degree has been achieved also by properly varying the heating

* Author for correspondence: paola.palmero@polito.it

1388–6150/$20.00

Akadémiai Kiadó, Budapest, Hungary
Springer, Dordrecht, The Netherlands

rate during firing [21]. However, in this investigation the dispersion was achieved by ball-milling, using α-alumina spheres, so that an even limited pollution from the milling media could have reasonably affected the crystallization temperature of α-alumina [22], the densification behavior and the microstructural evolution, also inducing a relevant grain growth in the final dense body [11].

As a matter of fact, in this paper also a well-dispersed, but un-polluted material, obtained by a prolonged magnetic stirring in aqueous medium, is investigated in terms of sintering behaviour and microstructural evolution. The aim of this paper is twofold: firstly, we optimized the heating rate during sintering for both nanostructured materials, precisely for the ball-milled and stirred samples.

Secondly, on the ground of the recent scientific literature [14], on the un-polluted material less conventional multi-steps sintering cycles have to be applied for a further retention of the primary particle size.

Experimental

A commercial, nanocrystalline transition alumina powder (NanoTek®, supplied by Nanophase Technology, USA, labelled as A) [23] was used in this study. A is characterized by crystallite size of about 50 nm, having spherical morphology; a full characterization of A is detailed in some previous papers [21, 24]. Water suspensions of A (7 vol.%) were submitted to granulometric analyses (Laser particle size analyzer Fritsch model Analysette 22 Compact) to determine the starting agglomerate size distribution. Aqueous slurries of A having a solid content of 50 mass% were then prepared by dispersion in distilled water, and the natural pH of 5.5 was achieved. De-agglomeration was performed under magnetic stirring (A_{MS}), performed for variable times up to 120 h, or by ball-milling (A_{BM}) up to 2.5 h, by using highly pure α-Al_2O_3 spheres (Bitossi, 2 mm in diameter). Ball-milling was carried out by using powder to spheres mass ratio of 1:10, at an angular velocity of 130 rpm, selected on the ground of literature data [25]. The degree of the agglomeration in the dispersed slurries was monitored by granulometric analyses.

Dried powders were ground into an agate mortar, sieved under 125 μm and uniaxially pressed at 300 MPa; the green densities of the bars were calculated from mass and geometrical measurements.

The sintering behaviour was investigated by dilatometric analyses (Netzsch 402E) performed up to 1500°C for 3 h. Different heating rates in the range 0.5–10°C min^{-1} were applied, whereas a cooling rate of 20°C min^{-1} was kept constant. Final densities were calculated by exploiting green densities, final mass and shrinkage data; the fired microstructures were characterised by SEM (Hitachi S2300) performed on fracture, un-treated surfaces.

In addition, on selected materials, sintering cycles, characterized by steps at variable heating rate (in the range 0.5–20°C min^{-1}), mainly starting in correspondence to some singular points detected on the previous dilatometric curves, were also tested.

Results and discussion

An extensive characterization of the powder A and of its classical, two-step linear shrinkage, during phase transformation and sintering was already discussed in some previous papers [21, 24]. After sintering at 1500°C for 3 h, the as-received A powder reached a poor fired density of about 2.86 g cm^{-3} (corresponding to 72% of the theoretical value, TD, of 3.987 g cm^{-3}). Dispersion was then performed prior of forming and sintering to improve fired ceramic quality.

Figure 1 shows the evolution of d_{50} values (which correspond to the 50% of the cumulative agglomerate size distribution, expressed by volume) as a function of the dispersion time. It clearly appears that 120 h of magnetic stirring as well as 2.5 h of ball-milling were necessary to reduce the starting agglomerate size of about one order of magnitude, thus to produce A_{BM} and A_{MS}, having almost superimposable agglomerate size distributions. In the insert, a zoom of the granulometric evolution of A_{BM} at short dispersion times is reported, showing similar d_{50} values after 2.5 or 4.5 h of milling. For limiting as much as possible the pollution of the sample from the milling media, dispersion was stopped after 2.5 h.

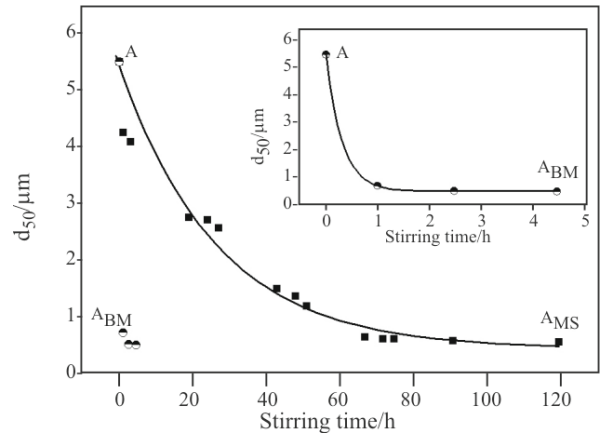

Fig. 1 Evolution of d_{50} values as a function of the dispersion time under magnetic stirring (A_{MS}) and ball-milling (A_{BM}). In the insert, zoom of the particle size evolution in A_{BM} samples

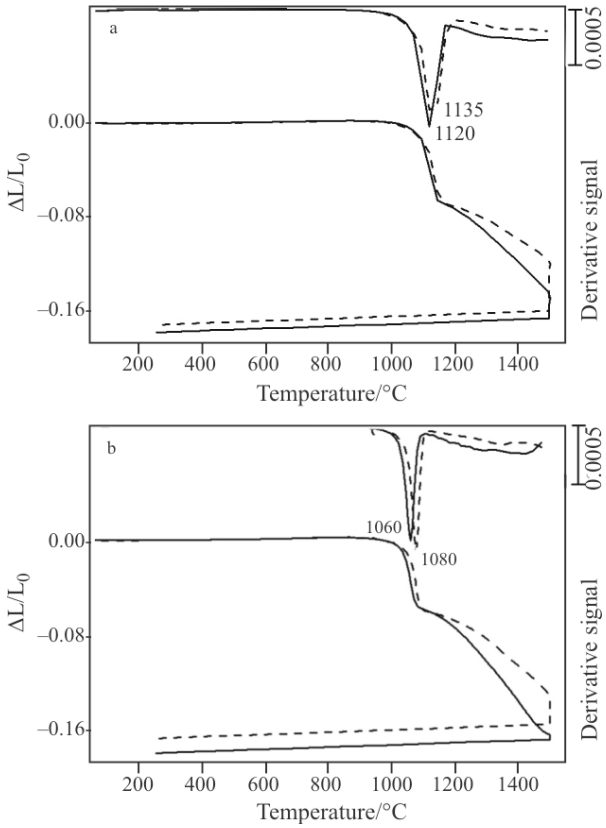

Fig. 2 Dilatometric analyses of A_{BM} (solid line) and A_{MS} (dashed line) up to 1500°C for 3 h; heating rate of a – 10 and b – 1°C min^{-1}

The dispersed powders were then pressed in bars, yielding A_{BM} and A_{MS} green bodies having similar density (about 2.15 g cm^{-3}). Figure 2a compares their dilatometric curves up to 1500°C for 3 h, with a heating rate of 10°C min^{-1}. They presented almost the same onset sintering temperature of about 1070°C. In contrast, a slight difference in $T_{0\rightarrow\alpha}$ value was shown by the derivative curves, since it was about 15°C lower in A_{BM}. This feature should be imputed to an expected seeding effect due to milling media, even if α-phase was undetectable by XRD. In addition, A_{BM} presented a more pronounced total linear shrinkage. In fact, in spite of the similar dilatomeric behaviour of the two materials during the first step, a larger linear shrinkage, achieved in a shorter time, was presented by A_{BM} during the second one, almost completely recovered by A_{MS} during its isothermal dwelling at 1500°C. Fired density of about 95.7 and 93.6% TD, respectively, were achieved.

The role of the dispersion route on the microstructural evolution was clearly evidenced by comparing the microstructures of A_{BM} and A_{MS} sintered bodies (Figs 3a and b). In fact, the ball-milled material was highly dense, but densification was accompanied by a significant grain growth. Its microstructure consists of well-facetted alumina grains of

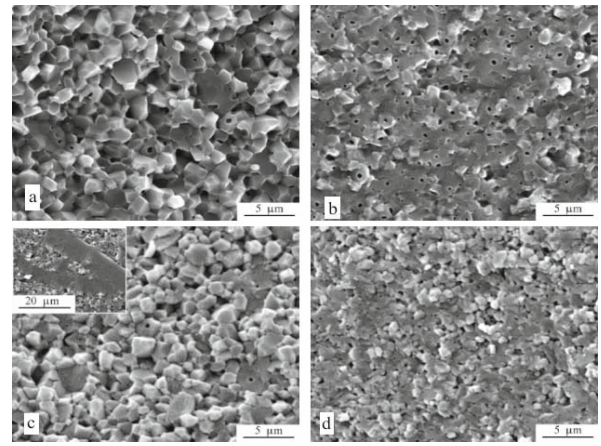

Fig. 3 SEM micrographs of a, c – A_{BM} and b, d – A_{MS} sintered at a, b – 10 or c, d – 1°C min^{-1} up to 1500°C for 3 h. In the insert of c, a region showing abnormal grain growth

about 2 μm in size, with a limited, residual porosity mostly located in intra-granular positions. A slight higher porosity was indeed observed in A_{MS}, characterized by a finer microstructure. The mean size of alumina grains was about 1–1.5 μm, entrapping mostly intra-granular, nanometric porosity.

For a further increase of the fired density, without inducing a relevant grain growth, the same dispersed materials were sintered up to 1500°C for 3 h, but lowering the heating rate to 1°C min^{-1}, on the ground of the recent literature [26], which states that a low heating rate induces, in the first shrinkage step, a lowering of the transformation temperature and a more effective particle rearrangement during phase transformation, and also increases the densification rate during the second one.

The densification curves of A_{BM} and A_{MS}, acquired at 1°C min^{-1}, are compared in Fig. 2 b. Once again, a slight displacement of the characteristic sintering temperatures between A_{MS} and A_{BM} was observed. In fact, the onset sintering temperatures were about 1025 and 1045°C, and the respective maximum transformation rate temperatures were located at 1060 and 1080°C, for A_{BM} and A_{MS}, respectively. As observed for the fast-heated samples, A_{BM} underwent a higher total linear shrinkage (18.3%) as compared to that of A_{MS} (17.2%), and once again the main differences in densification behaviour were observed during the second sintering step as well as during the isothermal dwell. In fact, in the second step, A_{BM} recorded a linear shrinkage of about 10.8%, reaching a very high densification degree (about 93% TD). As a consequence, a limited shrinkage of about 0.5% occurred during the isothermal treatment, yielding a final density of about 96.3% TD.

In contrast, A_{MS} recorded linear shrinkage of 7.5 and 2.5%, during the second step and the isothermal

dwell, respectively, leading to a fired body with a final density of 92.4% TD.

The fired microstructures of the above A_{BM} and A_{MS} materials are compared in Figs 3c and d. The prolonged duration of the thermal treatment of A_{BM}, due to the low heating rate, led to densification accompanied by abnormal grain growth. In fact, the high-density microstructure is made of well-facetted alumina grains, having a mean size of about 1.5–2 μm, near abnormally grown grains with sizes ranging from some micron to several tens of microns. In contrast, a very homogeneous microstructure was yielded in A_{MS} material, in which a certain amount of porosity, even if limited, should be still observed. The alumina particles present a narrow size distribution, ranging from 0.8 to 1 μm. On the ground of the above observations, the heating rate was further decreased to 0.5°C min^{-1}, and exploited for sintering the best performing material, i.e. A_{MS}.

Figure 4a compares the dilatometric curves of A_{MS} up to 1500°C for 3 h with heating rates of 10°C min^{-1} (solid line), 1°C min^{-1} (dashed line) and 0.5°C min^{-1} (dotted line), while the respective derivative curves are collected in Fig. 4b. By lowering the heating rate, the dilatometric curves were progressively displaced at lower temperatures. In fact, the onset sintering temperature was located at about 1070, 1045 and 1020°C for materials heated at 10, 1 and 0.5°C min^{-1}, respectively. Also the $T_{\theta\rightarrow\alpha}$ value was lowered from about 1135°C for the fast-fired sample to 1080 and 1060°C for the 1 and 0.5°C min^{-1}-sintered materials, respectively, as shown in Fig. 4b. Moreover, the first shrinkage step ranged from the onset sintering temperature up to 1180, 1100 and 1085°C for the 10, 1 and 0.5°C min^{-1}-fired samples. In contrast, the total linear shrinkage was almost unaffected by the heating rate since similar values were observed for the three A_{MS} samples. Just a slightly higher shrinkage was detected for the lowest heating sample, which reached a final density of about 94.8% TD. In addition, an opposite behaviour during the two steps was presented by the three materials as a function of the heating rate. In fact, during the first step, a slight decrease of linear shrinkage was recorded while lowering the heating rate. On the contrary, a significantly higher linear shrinkage in the second one was determined by decreasing the heating rate. Precisely, values of 5.12, 7.46 and 8.81% were recorded for samples heated at 10, 1 and 0.5°C min^{-1}, respectively. From Fig. 4b, a second peak of the derivative curves could be clearly detected in all the samples. The above signals reasonably correspond to the maximum densification rate temperature of α-alumina and once again, they are affected by the heating rate. In fact, they decrease from about 1370 to 1350°C and to 1315°C for the 10, 1 and 0.5°C-heated samples, respectively. This second inflection point was exploited for some other densification tests, as described in the followings.

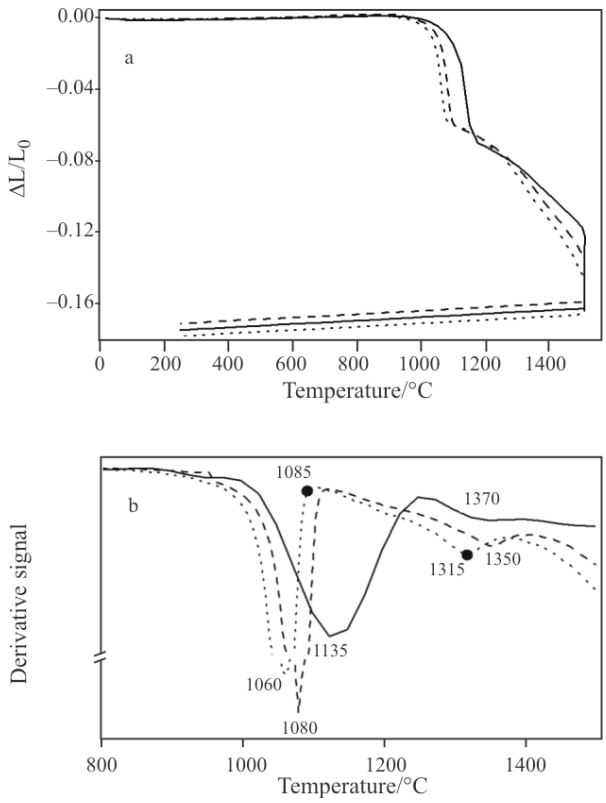

Fig. 4 a – Dilatometric and b – derivative curves of A_{MS} up to 1500°C for 3 h: heating rate of 10°C min^{-1} (solid line), 1°C min^{-1} (dashed line) and 0.5°C min^{-1} (dotted line)

In Fig. 5, the SEM micrograph of A_{MS} sintered at 0.5°C min^{-1} (a) up to 1500°C for 3 h is reported, and compared to those of materials fired at 1°C min^{-1} (b) and 10°C min^{-1} (c). It was clearly confirmed the effectiveness of lowering the heating rate in refining the final microstructure. In fact, the 0.5°C min^{-1}-fired

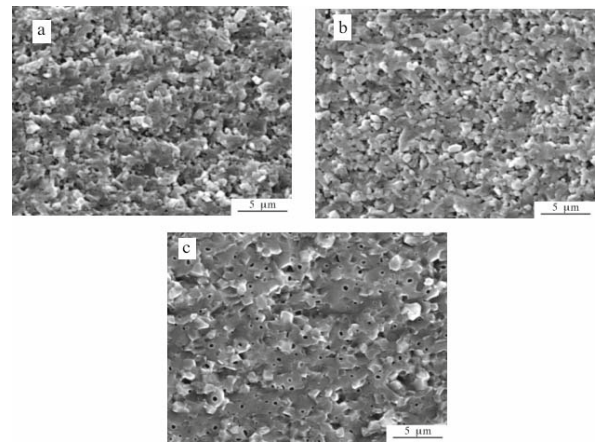

Fig. 5 SEM micrographs of A_{MS} sintered at a – 0.5, b – 1 or c – 10°C min^{-1} up to 1500°C for 3 h

material was characterized by a very homogeneous microstructure, with alumina grains with a mean size of about 0.7 μm, and by an ultra-fine, limited residual porosity.

In a previous paper [21], we observed that during the phase transformation a lower heating rate allows a better particles rearrangement, which promotes densification phenomena at high temperatures with a slight decrease of the residual porosity in final microstructures. On the other hand, tests performed at different heating rates did not imply a relevant limitation in alumina grains growth.

On the basis of these results, the A_{MS} materials were submitted to other sintering cycles performed at a heating rate of 0.5°C min^{-1}, but stopped at 1085°C ($A_{MS\text{-}1085}$), 1250°C ($A_{MS\text{-}1250}$), 1315°C ($A_{MS\text{-}1315}$), 1380°C ($_{AMS\text{-}1380}$), followed by a rapid cooling down to R.T. (at 20°C min^{-1}).

$A_{MS\text{-}1085}$ sample (Fig. 6a) showed a homogenous and well-packed microstructure made of very fine α-alumina particles, as stated by XRD analysis. A certain grain growth affected the $A_{MS\text{-}1250}$ material (Fig. 6b); an increase of the treatment temperature to 1315°C (Fig. 6c) or 1380°C (Fig. 6d) did not involve further relevant evolution in particles size.

Thus, two-step (TS) cycles were performed by increasing the heating rate from 0.5 to 20°C min^{-1} starting from 1085°C (sample labelled $A_{MS\text{-}TS\text{-}1085/1500}$) or 1315°C ($A_{MS\text{-}TS\text{-}1315/1500}$) up to 1500°C, with a dwell time of 3 h at the maximum temperature. The total linear shrinkage was slightly affected by the modification in heating rate, since values of 17.9, 17.5 and 16.7% were recorded by samples A_{MS}, $A_{MS\text{-}TS\text{-}1085/1500}$ and $A_{MS\text{-}TS\text{-}1315/1500}$, respectively. As a result, fired densities of about 93.5 and 91.0% TD were reached by the last two samples.

In Fig. 7, the fired microstructures of A_{MS}, $A_{MS\text{-}TS\text{-}1085/1500}$ and $A_{MS\text{-}TS\text{-}1315/1500}$ are reported.

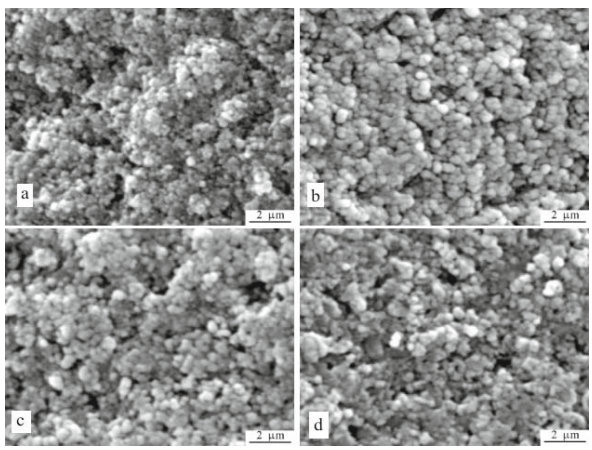

Fig. 6 SEM micrographs of A_{MS} sintered at a – 1085, b – 1250, c – 1315 and d – 1380°C (heating rate of 0.5°C min^{-1})

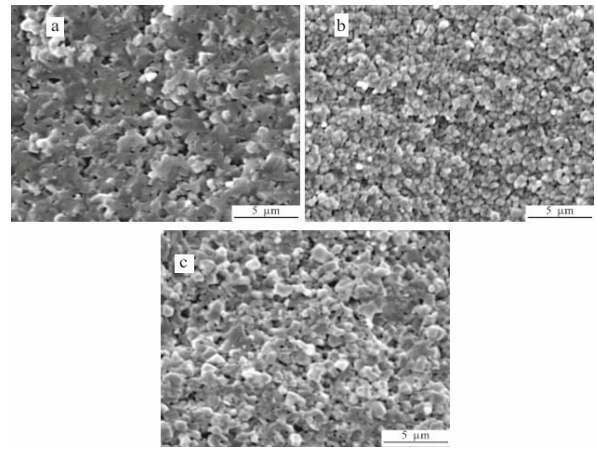

Fig. 7 SEM micrographs of a – A_{MS} heated at 0.5°C min^{-1}, b – $A_{MS\text{-}TS\text{-}1085/1500}$ and c – $A_{MS\text{-}TS\text{-}1315/1500}$ microstructures, all sintered at 1500°C for 3 h

It could be observed the significant refinement of $A_{MS\text{-}TS\text{-}1085/1500}$ microstructure, in which alumina grains were about 500 nm in size, as regards to the other materials, even if its fired density was lowered of about 1.5% TD with respects to A_{MS}.

To better understand the different microstructural evolution in $A_{MS\text{-}TS\text{-}1085/1500}$ and $A_{MS\text{-}TS\text{-}1315/1500}$ materials, a further two-step sintering treatment was performed, increasing the heating rate from 0.5°C to 20°C min^{-1} starting from 1085°C and stopping the heating step when the temperature of 1315°C was reached (labelled $A_{MS\text{-}TS\text{-}1085/1315}$). The $A_{MS\text{-}1315}$ and $A_{MS\text{-}TS\text{-}1085/1315}$ microstructures are compared in Fig. 8: both are highly homogeneous and made of α-alumina grains having a narrow size distribution. However, the fast-heating cycle resulted into a refinement of the mean grain size, from about 350 nm in $A_{MS\text{-}1315}$ (a) to about 250 nm in $A_{MS\text{-}TS\text{-}1085/1315}$ (b).

These results strengthened the conclusions of a previous paper [21], which stated that, during the sintering of a well-dispersed nano-crystalline powder, a low heating rate, in the temperature range in which phase transformation and particles rearrangement occurred, promotes the development of a well-packed, fine microstructure which can be maintained in the following densification at higher temperatures. However, this work demonstrated that if such low-heating rate is exploited also during the final sintering

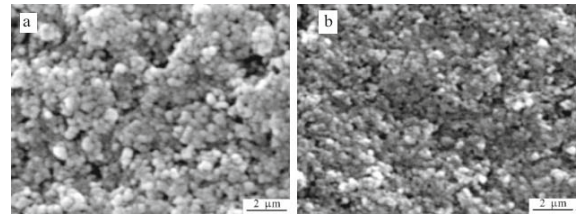

Fig. 8 SEM micrographs of a – $A_{MS\text{-}1315}$ and b – $A_{MS\text{-}TS\text{-}1085/1315}$

step, precisely in a critical temperature range, starting from 1085°C, a detrimental effect on microstructural evolution can be promoted, since a not negligible grain growth into the close-packed microstructures took place. As a matter of fact, the design of proper thermal cycles, able to promote densification avoiding any grain coarsening, can be successfully performed only if the overall phenomena taking place during both sintering steps are considered.

Conclusions

Well-dispersed suspensions of a transition nanocrystalline alumina were prepared both under prolonged magnetic stirring or by short-time ball-milling, performed with α-alumina spheres.

During pressureless sintering up to 1500°C, heating rate and dispersion route demonstrated to play a crucial role on densification and microstructural evolution. For ball-milled samples, a highly dense material was produced by lowering the heating rate from 10 to 1°C min^{-1}, but an abnormal grain growth affected the fired microstructure, probably also promoted by a certain α-alumina pollution from milling media. In contrast, a slight increase of the fired density and refinement of the microstructure in the stirred sample was achieved by decreasing the heating rate from 10 to 0.5°C min^{-1}.

In this last material, a crucial temperature range in which grains significantly grew was identified. A two-step sintering cycle, in which the heating rate was increased in the above range, was so exploited to achieve a further refinement of the fired microstructure, in spite of a slight decrease of the final density.

Acknowledgements

The authors wish to thank the European Commission for partially supporting this work in the framework of the Integrated Project 'NANOKER – Structural Ceramic Nanocomposites for top-end Functional Applications', contract no. NMP3-CT-2005-515784 (www.nanoker-society.org).

References

1 M. Crisan, A. Braileanu, D. Crisan, M. Raileanu, N. Dragan, D. Mardare, V. Teodorescu, A. Ianculescu, R. Birjega and M. Dumitru, J. Therm. Anal. Cal., 92 (2008) 7.
2 K. F. Cai, X. R. He and L. C. Zhang, Mater. Lett., 62 (2008) 1223.
3 H.-L. Wen and F.-S. Yen, J. Cryst. Growth, 208 (2000) 696.
4 F. S. Yen, H. L. Wen and Y. T. Hsu, J. Cryst. Growth, 233 (2001) 761.
5 C. S. Nordahl and G. L. Messing, J. Eur. Ceram. Soc., 22 (2002) 415.
6 S. J. Wu and L. C. De Jonghe, J. Am. Ceram. Soc., 79 (1996) 2207.
7 P. Bowen, C. Carry, D. Luxembourg and H. Hofmann, Powder Technol., 157 (2005) 100.
8 R.-J. Yang, F.-S. Yen, S.-M. Lin and C.-C. Chen, J. Cryst. Growth, 299 (2007) 429.
9 G. L. Messing and M. Kumagai, J. Am. Ceram. Soc., 73 (1994) 88.
10 J.-P. Ahn, J.-K. Park and H.-W. Lee, Nanostruct. Mater., 11 (1999) 133.
11 Z. P. Xie, J. W. Lu, L. C. Gao, W. C. Li, L. H. Xu and X. D. Wang, Mater. Design, 24 (2003) 209.
12 R.-J. Yang, F.-S. Yen, S.-M. Lin and C.-C. Chen, J. Cryst. Growth, 299 (2007) 429.
13 Z.-P. Xie, J.-W. Lu, Y. Huang and Y.-B. Cheng, Mater. Lett., 57 (2003) 2501.
14 V. R. Palkar, D. Thapa, M. S. Multani and S. G. Malghan, Mater. Lett., 36 (1998) 235.
15 H. Su and C. L. Johnson, J. Am. Ceram. Soc., 79 (1996) 3211.
16 K. An and D. L. Johnson, J. Mater. Sci., 37 (2002) 4555.
17 M. L. Huckabee and H. Palmour III, Am. Ceram. Soc. Bull., 51 (1972) 574.
18 I.-W. Chen and X.-H. Wang, Nature, 404 (2000) 168.
19 J. Li and Y. Ye, J. Am. Ceram. Soc., 89 (2006) 139.
20 R. Gadow and F. Kern, J. Ceram. Soc. Jpn., 114 (2006) 958.
21 P. Palmero, M. Azar, M. Lombardi, J. Chevalier, V. Garnier, G. Fantozzi and L. Montanaro, Int. J. Appl. Ceram. Technol., in press, DOI: 10.1111/j.1744-7402.2008.02281.x.
22 F. Lomello, P. Palmero, B. Bonelli, E. Garrone and L. Montanaro, J. Therm. Anal. Cal., DOI: 10.1007/s10973-008-9611-0.
23 http://www.nanophase.com
24 M. Azar, P. Palmero, M. Lombardi, V. Garnier, L. Montanaro, G. Fantozzi and J. Chevalier, J. Eur. Ceram. Soc., 28 (2008) 1121.
25 T. Doktor, P. Weymouth and T. Barson, Am. Ceram. Soc. Bull., 72 (1994) 54
26 D. Fargeot, D. Mercurio and A. Dauger, Mater. Chem. Phys., 24 (1990) 299

ICTAC 2008

DOI: 10.1007/s10973-008-9612-z